The Company of Biologists

RESEARCH ARTICLE

Mitotic checkpoint protein Mad1 is required for early Nup153 recruitment to chromatin and nuclear envelope integrity

Ikram Mossaid, Guillaume Chatel, Valérie Martinelli, Marcela Vaz and Birthe Fahrenkrog*,‡

ABSTRACT

Nucleoporin Nup153 is a multifunctional protein and a known binding partner of mitotic checkpoint protein Mad1 (also known as MAD1L1). The functional relevance of their interaction has remained elusive. Here, we have further dissected the interface and functional interplay of Nup153 and Mad1. Using *in situ* proximity ligation assays, we found that the presence of a nuclear envelope (NE) is a prerequisite for the Nup153–Mad1 association. Time-lapse microscopy revealed that depletion of Mad1 delayed recruitment of Nup153 to anaphase chromatin, which was often accompanied by a prolongation of anaphase. Furthermore, as seen by electron microscopic and three-dimensional structured illumination investigations, Nup153 and Mad1 depletion led to alterations in NE architecture, characterised by a change of membrane curvature at nuclear pore complexes (NPCs) and an expansion of the spacing between inner and outer nuclear membranes. Nup153 depletion, but not Mad1 depletion, caused defects in interphase NPC assembly, with partial displacement of cytoplasmic nucleoporins and a reduction in NPC density. Taken together, our results suggest that Nup153 has separable roles in NE and NPC formation: in post-mitotic NE re-formation in concert with Mad1 and in interphase NPC assembly, independent of Mad1.

KEY WORDS: Nuclear pore complex assembly, Mitotic checkpoint, Nup153, Mad1

INTRODUCTION

Nuclear pore complexes (NPCs) are large multiprotein complexes that accomplish all macromolecular exchange across the nuclear envelope (NE). NPCs consist of multiple copies of ∼30 different nucleoporins (Nups) that assemble into several biochemically and structurally defined entities: the NPC scaffold, an assembly of distinct ring moieties, the cytoplasmic filaments and the nuclear basket (Beck and Hurt, 2017; Hoelz et al., 2016; Knockenhauer and Schwartz, 2016; Schwartz, 2016). Major building blocks of the NPC scaffold are the Nup107–160 complex (also known as the Y-complex), which is composed of nine nucleoporins, and the five-nucleoporin-comprising Nup93 complex. Both the Nup107–160 and the Nup93 complex are critical for NPC assembly (Boehmer et al., 2003; Hawryluk-Gara et al., 2008; Sachdev et al., 2012; Souquet et al., 2018; Vollmer and Antonin, 2014; Vollmer et al., 2012; Walther et al., 2003). Cytoplasmic filaments and the nuclear basket are predominantly made of phenylalanine-glycine (FG)-repeat-containing nucleoporins, which are of particular importance for nucleocytoplasmic transport (Lim et al., 2008; Patel et al., 2007; Terry and Wente, 2009). One such FG-repeat nucleoporin is Nup153, a constituent of the nuclear basket (Fahrenkrog et al., 2002; Pante et al., 2000; Walther et al., 2001). Nup153 is a multifunctional protein with roles that go well beyond nucleocytoplasmic transport (Ball and Ullman, 2005; Duheron et al., 2017; Lemaitre et al., 2012; Lussi et al., 2010; Mackay et al., 2009, 2017; Moudry et al., 2012; Nanni et al., 2016; Prunuske et al., 2006; Toda et al., 2017; Vaquerizas et al., 2010; Zhou and Pante, 2010). In this regard, Nup153 is known to play a role in both post-mitotic and interphase NPC assembly.

Post-mitotic NPC assembly is initiated as early as anaphase, and the first nucleoporins that accumulate on chromatin are members of the Nup107–160 complex, followed by a small fraction of Nup153 and its nuclear basket partner Nup50 (Anderson et al., 2009; Dultz et al., 2008; Schwartz et al., 2015; Vagnarelli and Earnshaw, 2012). Nup107–160 complex recruitment is mediated by ELYS (also known as Mel-28 and AHCTF1), which associates to chromatin via its AT-hook DNA-binding motif (Fernandez and Piano, 2006; Franz et al., 2007; Lau et al., 2009; Rasala et al., 2008; Walther et al., 2003). Recruitment of Nup153 onto chromatin occurs independently of ELYS, and Nup153 may substitute for ELYS to recruit the Nup107–160 complex (Schwartz et al., 2015). Nup153 is capable of recruiting a large number of nucleoporins from basically all NPC substructures (Bilir et al., 2019; Dultz et al., 2008; Schwartz et al., 2015; Walther et al., 2001), indicating that it is able to seed the formation of NPCs on chromatin (Schwartz et al., 2015). Important for targeting Nup153 to anaphase chromatin is a complex between Repo-Man (also known as CDCA2) and importin β (KPNB1; Vagnarelli and Earnshaw, 2012; Vagnarelli et al., 2011). Lack of Repo-Man impairs importin β recruitment and subsequent recruitment of Nup153 to the anaphase chromatin. Whether Repo-Man docks to the chromatin directly or indirectly remains unclear (Vagnarelli and Earnshaw, 2012).

Interphase NPC assembly occurs into a closed NE as cells progress through interphase (Maul et al., 1971; Otsuka and Ellenberg, 2018) and it requires the Nup107–160 complex (D'Angelo et al., 2006; Doucet and Hetzer, 2010; Doucet et al., 2010; Harel et al., 2003; Walther et al., 2003). Similarly, the transmembrane nucleoporin POM121 and Nup153 are necessary (Talamas and Hetzer, 2011; Vollmer et al., 2015), but not so ELYS (Doucet et al., 2010). Interphase NPC assembly requires an insertion into the nuclear membrane and fusion of the outer nuclear membrane (ONM) and the inner nuclear membrane (INM). Nup153 can interact with the INM via an N-terminal amphipathic helix, and Nup153 insertion into the INM facilitates the recruitment of the Nup107–160 complex to these NPC assembly sites (Vollmer et al., 2015). Likewise, Nup1, the yeast paralogue of Nup153, induces membrane curvature by amphipathic helix insertion into the lipid bilayer (Meszaros et al., 2015). The interaction of Nup153 with

the INM is regulated by its nuclear import receptor transportin 1 (TNPO1) and by the GTP-bound form of the small GTPase Ran (Vollmer et al., 2015).

Mad1 (also known as MAD1L1) is a key component of the mitotic checkpoint [also termed the spindle assembly checkpoint (SAC)], which delays anaphase onset until all chromosomes have been properly attached to the mitotic spindle. Mad1 localises to NPCs in interphase (Campbell et al., 2001; Iouk et al., 2002; Lussi et al., 2010), where it binds the two nuclear basket nucleoporins Tpr and Nup153 (Ding et al., 2012; Lee et al., 2008). The association of Mad1 with Tpr plays an important role in mitotic checkpoint regulation (Cunha-Silva et al., 2020; Lee et al., 2008; Lopez-Soop et al., 2017; Rajanala et al., 2014; Rodriguez-Bravo et al., 2014; Schweizer et al., 2013), whereas the functional significance of the Mad1–Nup153 complex has remained largely elusive. Here we provide evidence that Mad1 is required for seeding Nup153 on anaphase chromatin and post-mitotic NPC assembly.

RESULTS
Mad1 exhibits two independent binding sites for Nup153
We have previously shown that Nup153 and Mad1 directly interact, both *in vitro* and *in situ*, and that the N-terminal domain of Nup153 establishes binding to Mad1 (Lussi et al., 2010). To deepen the analysis of the Nup153–Mad1 interface and to identify the region of Mad1 that binds Nup153, we carried out GST pulldown assays. To do so, we expressed distinct Mad1 fragments fused to a FLAG tag (Fig. 1A) and the N-terminal part of Nup153 fused to GST (residues 2–610; GST–153N; Lussi et al., 2010) in *E. coli*. GST alone was used as negative control. Coomassie Blue-stained SDS gels showing the input used for the pulldown assays are shown in Fig. S1. As shown in Fig. 1B, full-length FLAG–Mad1 (Mad1) and the N-terminal domain of Mad1 (residues 1–596; N596) bound to GST–Nup153, but not to GST. The C-terminal domain of Mad1 (CTD; residues 597–718, C597–718) showed no interaction with GST–Nup153. A further dissection of the N-terminal domain of Mad1 revealed that the Mad2-interacting motif (MIM) of Mad1 (N539) is dispensable for binding Nup153 (Fig. 1C) and that residues 121–240 of Mad1 (N121–240) are sufficient for Nup153 binding (Fig. 1D). Consequently, Mad1 residues 1 to 240 (N240; Fig. 1C) bound Nup153, in contrast to fragments comprising residues 1–120 (N120) and residues 241–539 (N241–539; Fig. 1D). These findings are in good agreement with a previous study that showed that residues 1–274 are necessary and sufficient for the localisation of Mad1 at NPCs (Rodriguez-Bravo et al., 2014).

We further identified a second Nup153-binding site in the N terminus of Mad1: residues 241–596, 540–718 and 552–718 of Mad1 did bind GST–153N (Fig. 1D,E), but residues 597–718 did not (Fig. 1B,E). We therefore concluded that the N-terminal domain of Mad1 comprises two binding sites for Nup153: one involving residues 121–240 and the second involving residues 552–596.

Nup153 and Mad1 convene exclusively in the presence of the NE
Although Nup153 and Mad1 colocalise at NPCs during interphase (Lussi et al., 2010), they adopt different locations during mitosis: Nup153 is found dispersed in the mitotic cytoplasm (Dultz et al., 2008; Mackay et al., 2009), whereas Mad1 is localised to unattached kinetochores during prophase and prometaphase to fulfil its SAC function (Chen et al., 1998). To further characterise the association between Nup153 and Mad1 in space and time in cells, we next performed *in situ* proximity ligation assays (PLA) in HeLa cells (see Materials and Methods; Soderberg et al., 2006). Abundant PLA

signals at the edge of the nucleus (visualised by DAPI staining) were detected in interphase cells (Fig. 2A). PLA signals were diminished upon depletion of Nup153 or Mad1 (Fig. 2A,B). Depletion of Tpr, another nucleoporin known to bind Mad1 (Lee et al., 2008), had no impact on the Nup153–Mad1 PLA signals (Fig. 2A,B), suggesting that the Nup153 and Mad1 interaction is independent of Tpr. PLA results were validated using different control pairs (Fig. S2A,B). Knockdown efficiency for the distinct siRNAs was determined using western blotting (Fig. S2C,D).

Having confirmed the association between Nup153 and Mad1 at the NE, we next asked whether Nup153 and Mad1 show some association during mitosis, which may have previously escaped detection by conventional immunofluorescence microscopy. We performed PLA assays in HeLa cells stably expressing YFP–tubulin to precisely monitor the cell cycle state. As shown in Fig. 2C, PLA signals for Nup153 and Mad1 were only visible in the presence of the NE. Quantification of the PLA signals for each cell cycle state revealed that PLA signals were established in telophase (when the NE is forming), increased during cytokinesis (when NE formation is completed), remained during interphase and declined in prophase (when the NE begins to disassemble) (Fig. 2D). Consistent with these data, we observed no significant PLA signal between Nup153 and Mad1 during prometaphase in normal HeLa cells (Fig. S2B). Additionally, no PLA signal between Nup153 and the outer kinetochore protein Hec1 (also known as NDC80; Wei et al., 2005) was observed during prometaphase, in contrast to Mad1 and Mad2 (Fig. S2B). Taken together these data confirm the absence of Nup153 from mitotic structures (Mackay et al., 2009) and they suggest a dissociation of the Nup153–-Mad1 complex at the beginning of the mitosis when the NE disassembles.

Mad1 is required for Nup153 recruitment to the re-forming NE
We previously reported that overexpression of Nup153 causes a SAC override, whereas depletion of Nup153 has no obvious impact on SAC function (Lussi et al., 2010). This observation was confirmed by observations of decreasing phospho-histone H3 levels, timely cyclin B1 and securin degradation (Fig. S3A), as well as timely Cdc20 dissociation from Mad2 in Nup153-depleted cells after release from nocodazole arrest (Fig. S3B). Because of a missing apparent effect of Nup153-depletion on Mad1 and SAC function, we next assessed whether Mad1-depletion impacts Nup153. In immunofluorescence experiments, we found that the recruitment of Nup153 to chromatin in anaphase was compromised in the absence of Mad1 (Fig. 3A). However, the localisation of Nup153 in any other cell cycle phase was indistinguishable between control and Mad1-depleted cells (Fig. 3A). Quantification of the fluorescence intensity revealed that the Nup153 signal increased twofold from interphase to anaphase in control cells, but not in Mad1-depleted cells, when normalised to the respective interphase intensity (Fig. 3B). Fluorescence intensities in telophase/ cytokinetic cells were similarly stronger in control and Mad1-depleted cells. When the signal for the respective cell cycle state was normalised to the intensity of control cells, Nup153 intensity was slightly stronger in Mad1-depleted interphase and telophase/ cytokinetic cells, but decreased in anaphase cells (Fig. 3C). The effect of Mad1 depletion on Nup153 recruitment to anaphase chromatin appeared specific: in the absence of Mad1, neither anaphase recruitment of importin β to chromatin (Fig. S4A–C; see also Vagnarelli et al., 2011) nor Tpr recruitment in late telophase (Fig. S4D,E) was altered.

Time-lapse imaging in HeLa T-Rex cells conditionally expressing GFP–Nup153 (Duheron et al., 2014) confirmed the
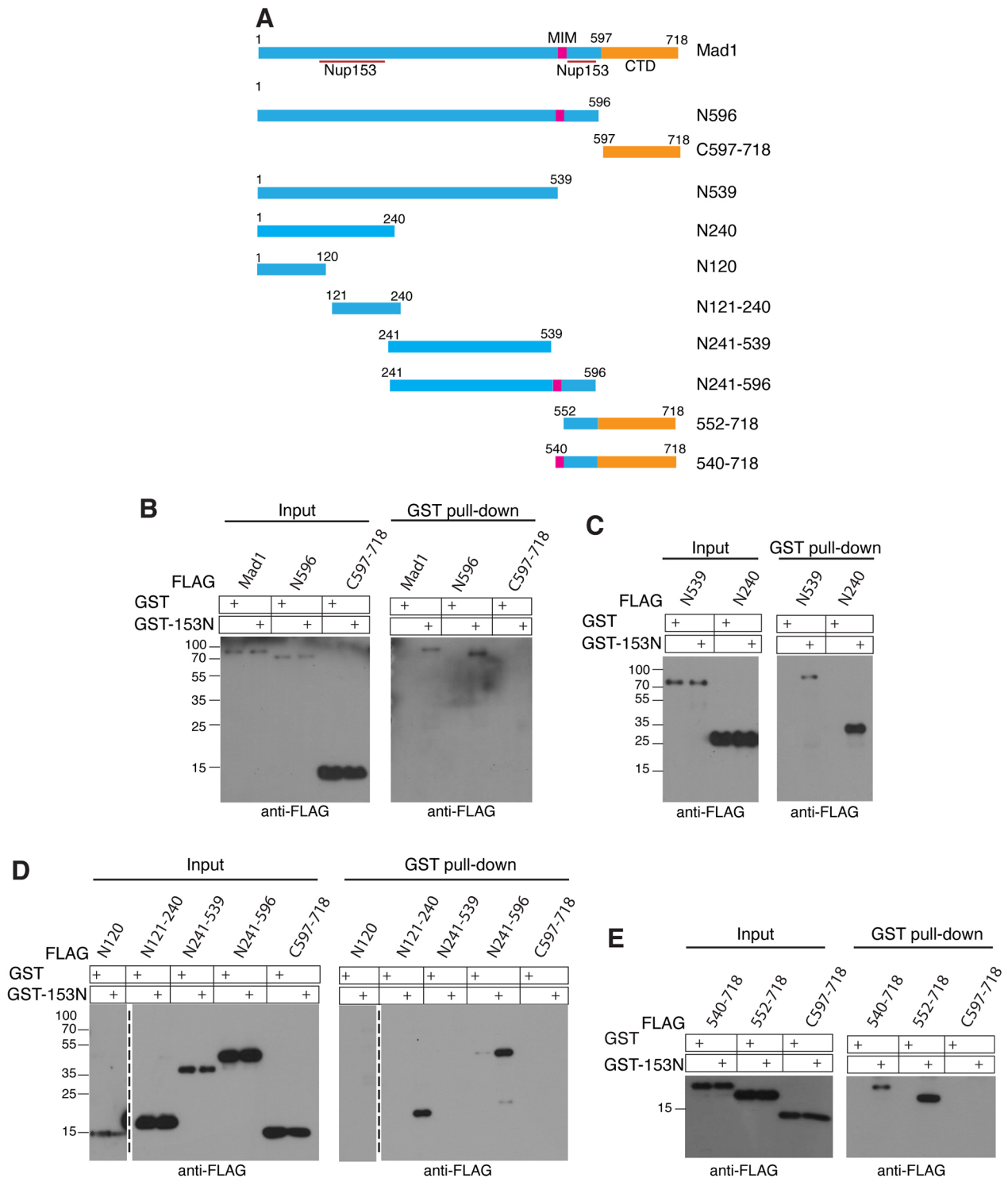
Fig. 1. Mad1 has two independent binding sites for Nup153. (A) Schematic representation of Mad1 fragments used for binding assays. (B) GST pulldown assays were performed using recombinant GST–Nup153N (GST–153N, residues 2–610) and GST alone. Recombinant FLAG-tagged Mad1 fragments comprised full-length Mad1, a fragment of the N-terminal domain (residues 1–596; N596) and a fragment of the C-terminal domain (residues 597–718; C597–718). Input and bound fractions (GST pull-down) were analysed by immunoblotting using anti-FLAG antibodies. Analysis of the interaction between Nup153 and shorter N-terminal fragments of Mad1 comprising (C) residues 1–539 (N539) and residues 1–240 (N240), and (D) residues 1–120 (N120), residues 121–240 (N121–240), residues 241–539 (N241–539) and residues 241–596 (N241–596). Nup153 interacts with residues 1–240, the N121–240 fragment and the N241–596 fragment of Mad1. (E) GST pulldown using Mad1 fragments spanning residues 540–718, residues 552–718 (lacking the MIM domain) and residues 597–718 (C597–718). Mad1 residues 552–596 mediate the interaction with Nup153.

necessity of Mad1 for Nup153 recruitment to anaphase chromatin. Cells were imaged every minute from anaphase to cytokinesis (representative images are shown in Fig. 3D). Although

GFP–Nup153 appeared on chromatin within 5 min (Fig. 3D, white asterisk) of anaphase onset in control cells, it took about 7 min in Mad1-depleted cells (Fig. S5A). This significant delay in Nup153
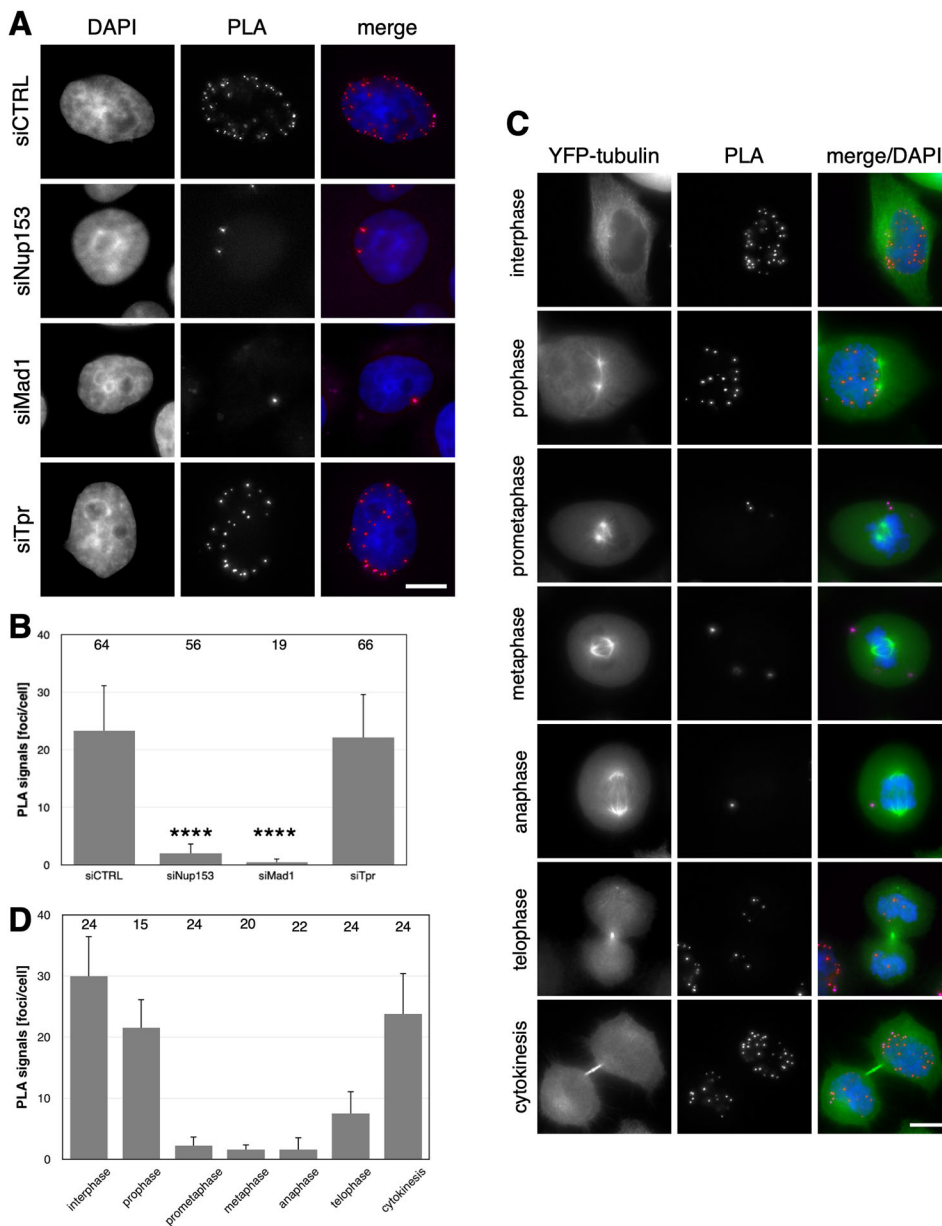
Fig. 2. Proximity ligation assays reveal a nuclear envelope-dependent association between Nup153 and Mad1. (A) HeLa cells were treated with the indicated siRNAs for 48 h (siTpr for 72 h; siCTRL, control non-targeting siRNA) and labelled with primary anti-Nup153 and anti-Mad1 antibodies followed by secondary oligonucleotide-linked probes to generate the PLA signal. DNA was visualised using DAPI (blue). Representative epifluorescence images are shown. Scale bar: 10 µm. (B) Quantification of Nup153–Mad1 PLA foci per cell after treatment with the indicated siRNAs. Total numbers of analysed cells per condition are indicated at the top of the graph. Values are mean±s.d. ****$P<0.0001$; t-test, two-tailed. (C) HeLa cells stably expressing YFP–tubulin subjected to *in situ* PLA at different cell cycle states using anti-Nup153 and anti-Mad1 antibodies. PLA association (red) between Nup153 and Mad1 occurs primarily from telophase to prophase (i.e. in the presence of a nuclear envelope). Representative epifluorescence images are shown. DNA was visualised using DAPI (blue). Scale bar: 10 µm. (D) Quantification of Nup153–Mad1 PLA foci for the distinct cell cycle states. Total numbers of analysed cells per condition are indicated at the top of the graph. Values are mean±s.d.

recruitment often coincided with an elongation of anaphase (Fig. 3D, red line) and was observed in ~33% of Mad1-depleted cells, but only in ~7% of control cells (Fig. 3E). Mad2 depletion, on the contrary, had no effect on Nup153 recruitment to chromatin in anaphase (Fig. 3D,E) or the duration of anaphase (Fig. 3D; Fig. S5A). Similarly, Mad1 depletion had no effect on the recruitment of GFP–Nup98 to the re-forming NE, that is, 1–2 min after the end of anaphase (Fig. S5B), despite the significant prolongation of anaphase in Mad1-depleted cells (Fig. S5A,B), indicating that the effect of Mad1 depletion on Nup153 recruitment is specific.

Nup153 and Mad1 are required for nuclear envelope integrity

We next performed electron microscopy analysis of Nup153- and Mad1-depleted HeLa cells. Strikingly, the space between outer and inner nuclear membrane, the perinuclear space (PNS), was significantly increased in Nup153- and Mad1-depleted cells as compared to the PNS in control cells (Fig. 4A,B). Furthermore, we noticed that the membrane curvature at NPCs was reduced in

Nup153- and Mad1-depleted cells (Fig. 4B, black arrow). The PNS increased from ~40–50 nm in control cells to ~80–100 nm in Nup153- and Mad1-depleted cells (Fig. 4C). PNS spacing and membrane curvature remained unaffected by the depletion of Nup50, a Nup153 binding partner at the nuclear basket (Duheron et al., 2014), as well as by the depletion of the three cytoplasmic-located nucleoporins Nup358 (also known as RANBP2), Nup214 and Nup88 (Fig. S6A,B). Depletion of Tpr, the third nucleoporin of the nuclear basket, led to a significant increase in the perinuclear space (Fig. S6B), although to a lesser extent than the increase in Nup153- and Mad1-depleted cells. This might be due to an indirect effect, because Mad1 recruitment to NPCs is partially impaired in the absence of Tpr (Lee et al., 2008; Schweizer et al., 2013). We confirmed the dilation of the PNS upon depletion of Nup153 and Mad1 using three-dimensional structured illumination microscopy (3D-SIM). The ONM was visualised using anti-nesprin-2 antibodies (Fig. 4D, green) and the INM by anti-lamin A/C antibodies (Fig. 4D, red). Whereas both signals appeared in the
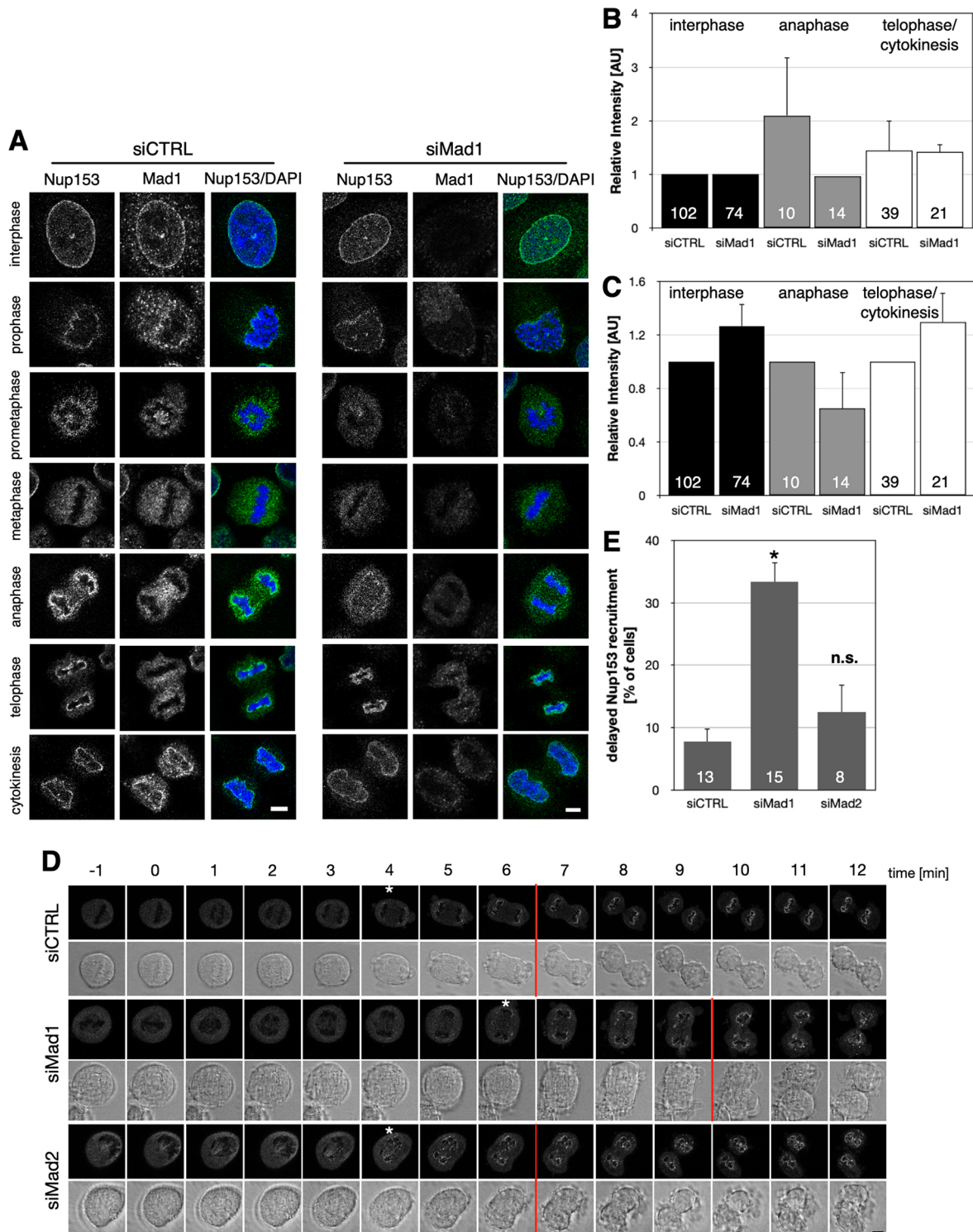
Fig. 3. Mad1 depletion delays recruitment to chromatin in anaphase. (A) HeLa cells were transiently transfected with the indicated siRNAs (siCTRL, control non-targeting siRNA), labelled with anti-Nup153 and anti-Mad1 antibodies and analysed by confocal laser-scanning microscopy. In Mad1-depleted cells, Nup153 recruitment to chromatin is delayed. DNA was visualised using DAPI (blue). Scale bars: 5 µm. Quantification of the fluorescence intensity (AU, arbitrary units) of Nup153 at different cell cycle stages in siCTRL- and siMad1-treated cells with normalisation to (B) the respective interphase intensity for each treatment and (C) the intensity in control cells at each cell cycle state. Total number of analysed cells per condition is indicated at the bottom of each bar. Values are mean±s.d. (D) HeLa T-Rex cells expressing GFP–Nup153 were transiently transfected with the indicated siRNAs and subjected to live-cell imaging 48 h after transfection. Imaging started two minutes (time −1) before anaphase onset (time 1) using confocal laser-scanning microscopy. Images were taken every minute from the last time point before anaphase onset. White asterisks indicate the first evidence of Nup153 recruitment to the condensed chromatin, red bars the onset of telophase (i.e. the first indication of the cleavage furrow). Differential interference contrast and confocal images are shown. Scale bar: 5 µm. (E) Quantification of cells exhibiting a delay of Nup153 recruitment to chromatin. Total number of analysed cells per condition is indicated at the bottom of each bar. Values are mean±s.d. *P<0.05; n.s., not significant; t-test, two-tailed.
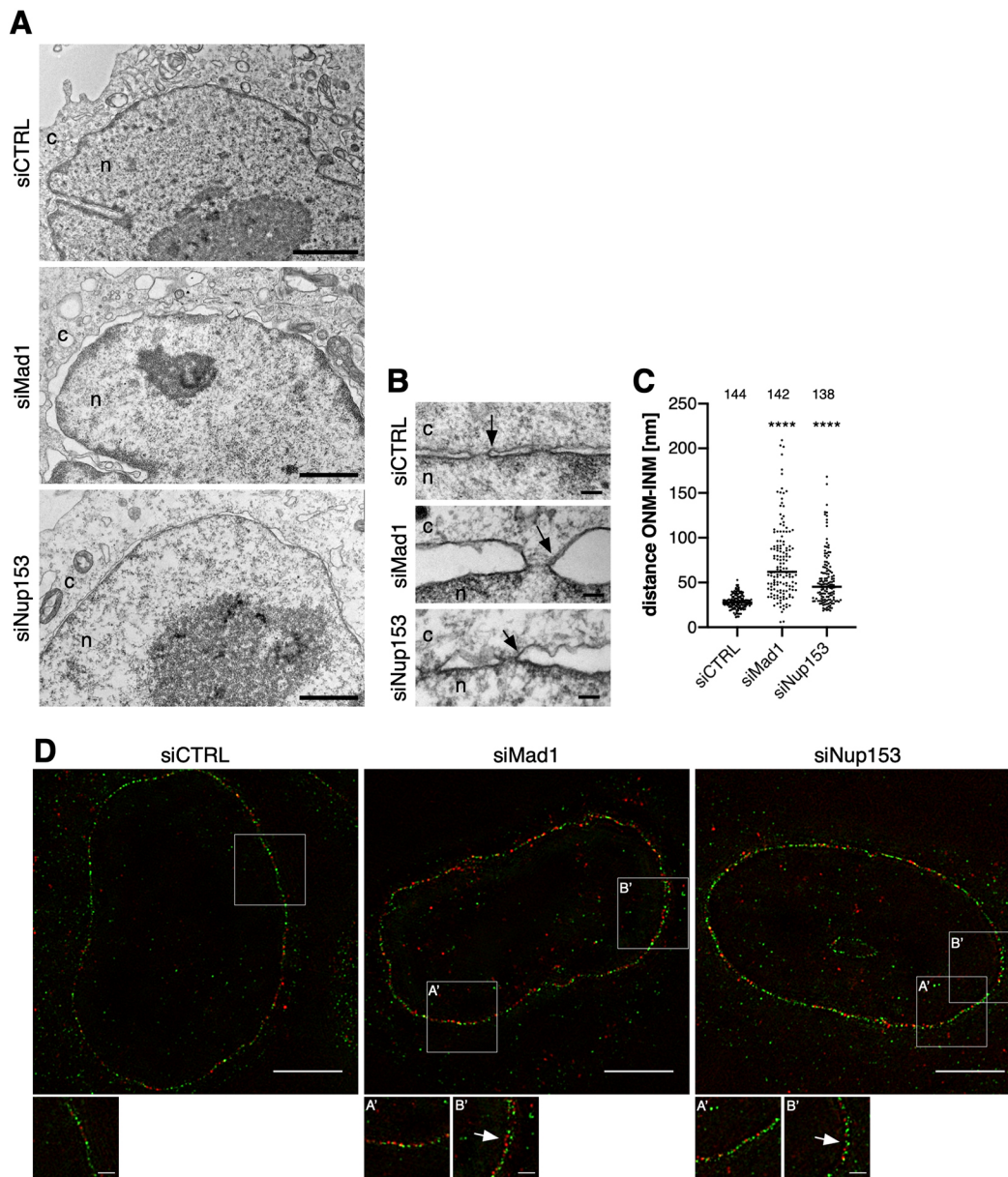
Fig. 4. Nup153 and Mad1 depletion induces nuclear envelope anomalies. (A) HeLa cells were treated with the indicated siRNAs (siCTRL, control non-targeting siRNA) for 48 h and prepared for thin-section electron microscopy. Cross-sections of the NE are shown. (B) NE cross-section at higher magnification. The perinuclear space is enlarged in Mad1- and Nup153-depleted cells, and membrane curvature is altered (black arrows). Scale bars: 500 nm in A, 100 nm in B. n, nucleoplasm; c, cytoplasm. (C) Quantification of the spacing between ONM and INM of Nup153- and Mad1-depleted cells. The distance between outer and inner nuclear membrane was measured adjacent to NPCs, using ImageJ. Total number of measurements are indicated at the top of each plot. Mean values are represented by horizontal lines. ****$P<0.0001$; unpaired two-tailed t-test. (D) HeLa cells transiently transfected with Nup153 and Mad1 siRNAs, stained with antibodies against nesprin-2 (green) and lamin A/C (red), and analysed using 3D-SIM. Zoom-in images of the highlighted areas (boxes) show the increased distance between nesprin-2 and lamin A/C signals (white arrows) upon depletion of Nup153 and Mad1. Scale bars: 5 μm, insets 1 μm.

same focal plane in control cells, green and red signals were partially separated in the absence of Nup153 or Mad1, indicating a spacing of the two membranes of more than 100 nm (the optical resolution of SIM). This increase in spacing between the ONM and the INM, however, appeared to have no effect on the localisation of nuclear membrane proteins, as indicated by normal NE localisation of Sun1 (at the ONM) and nesprin-2 (at the INM; Fig. S6C).

Nup153, but not Mad1, is required for NPC integrity

In yeast, Nup1, the functional homologue of Nup153, is known to bind to the NE and to regulate membrane curvature due to an

amphipathic helix in its N-terminal part (Meszaros et al., 2015). This helix, which is able to interact with lipids, is implicated in the membrane remodelling process, and deletion of this N-terminal part of Nup1 provokes a reduction in membrane curvature. This reduced membrane curvature coincides with a partial mislocalisation of the yeast cytoplasmic nucleoporins Nup159 and Nup82 (Meszaros et al., 2015). We wondered whether the reduction in membrane curvature observed in Nup153-depleted HeLa cells would alter cytoplasmic nucleoporins in mammalian cells as well. We therefore monitored the localisation of the cytoplasmic ring nucleoporins Nup214 (orthologue of the yeast

Nup159) and Nup88 (orthologue of the yeast Nup82) as well as the mammalian cytoplasmic filament protein Nup358 using immunofluorescence microscopy. As shown in Fig. 5A, Nup153 depletion led to a partial displacement of Nup214, Nup88 and Nup358 from the NPCs and to their accumulation in cytoplasmic foci. Mad1 depletion, on the contrary, did not alter the localisation of the three cytoplasmic nucleoporins (Fig. 5B).

Furthermore, we extended this analysis to mouse 3T3 fibroblast cells, to investigate whether the effect of the depletion of Nup153 is conserved in mammalian cells. In a manner similar to HeLa cells, we detected a mislocalisation of Nup214 and Nup358 in Nup153-depleted 3T3 cells (Fig. 6). To confirm that this effect was specifically caused by Nup153 depletion, we next carried out rescue experiments by expressing human GFP–Nup153 in control and Nup153-depleted 3T3 cells. Human and mouse Nup153 share 83% sequence identity at the protein level (www.ncbi.nlm.nih.gov/homologene). As shown in Fig. 6A, Nup214 and Nup358 accumulated in cytoplasmic foci in control and Nup153-depleted 3T3 cells expressing GFP, whereas expression of human GFP–Nup153 restored localisation of Nup214 and Nup358 to NPCs in Nup153-depleted 3T3 cells, and the cytoplasmic foci did not appear (Fig. 6B). Cytoplasmic foci were only seen in neighbouring cells that did not express human GFP–Nup153. Depletion of endogenous mouse Nup153 and expression of human GFP–Nup153 was confirmed using western blot analysis (Fig. 6C). Taken together, our data suggest that Nup153 may play an essential, conserved function in NPC assembly in mammalian cells, similar to its function in yeast.

Nup153 depletion affects NPC assembly in interphase cells

Having seen that depletion of Nup153 leads to a partial mislocalisation of the cytoplasmic nucleoporins, we next investigated whether this defect results from a defect in interphase NPC assembly or at the end of mitosis. Interphase NPC assembly occurs after DNA replication in S phase. We therefore arrested cells before entry into mitosis at the G2-M boundary by treatment with the CDK1 inhibitor RO-3306. Non-synchronised and arrested cells were stained with NPC-specific mAb414 antibodies, which recognise nucleoporins containing FG repeats. As shown in Fig. 7A and quantified in Fig. 7B, NPC density was significantly reduced in RO-3306-arrested, Nup153-depleted cells. Mad1 depletion, on the contrary, did not affect NPC density, suggesting that Nup153, but not Mad1, is required for interphase NPC assembly.

DISCUSSION

We previously identified the spindle checkpoint protein Mad1 as binding partner of Nup153 (Lussi et al., 2010). In this study, we confirm this interaction and establish a role for Mad1 in Nup153 recruitment to chromatin in anaphase and in post-mitotic NPC assembly.

Our previous study has shown that the N-terminal domain of Nup153 binds Mad1 (Lussi et al., 2010). Mad1 comprises two independent binding sites for this N-terminal region of Nup153: the first region involves residues 121–240, the second region involves residues 552–596 (Fig. 1). Residues 121–240 overlap with the previously described NPC targeting domain of Mad1 (residues 1–274), which mediates its interaction with Tpr (Rodriguez-Bravo et al., 2014). Residues 552–596 are located to the C-terminal side of
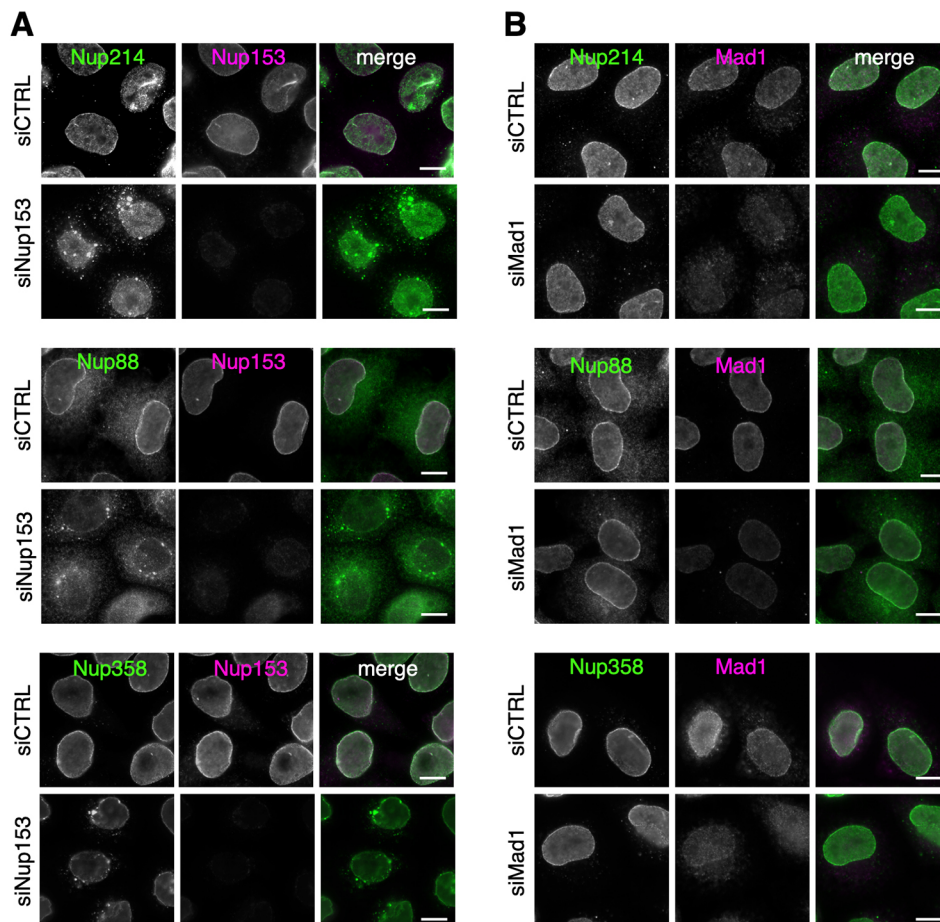

Fig. 5. Partial displacement of cytoplasmic nucleoporins from NPCs upon Nup153 depletion. (A) siRNA-mediated depletion of Nup153 causes a partial displacement of Nup88, Nup214 and Nup358 to foci in the cytoplasm, in contrast to (B) Mad1 depletion. HeLa cells were treated with the indicated siRNAs (siCTRL, control non-targeting siRNA) and labelled with anti-Nup214, anti-Nup88 and anti-Nup358 antibodies (green) and co-stained with anti-Nup153 or anti-Mad1 antibodies (magenta). Scale bars: 10 µm.
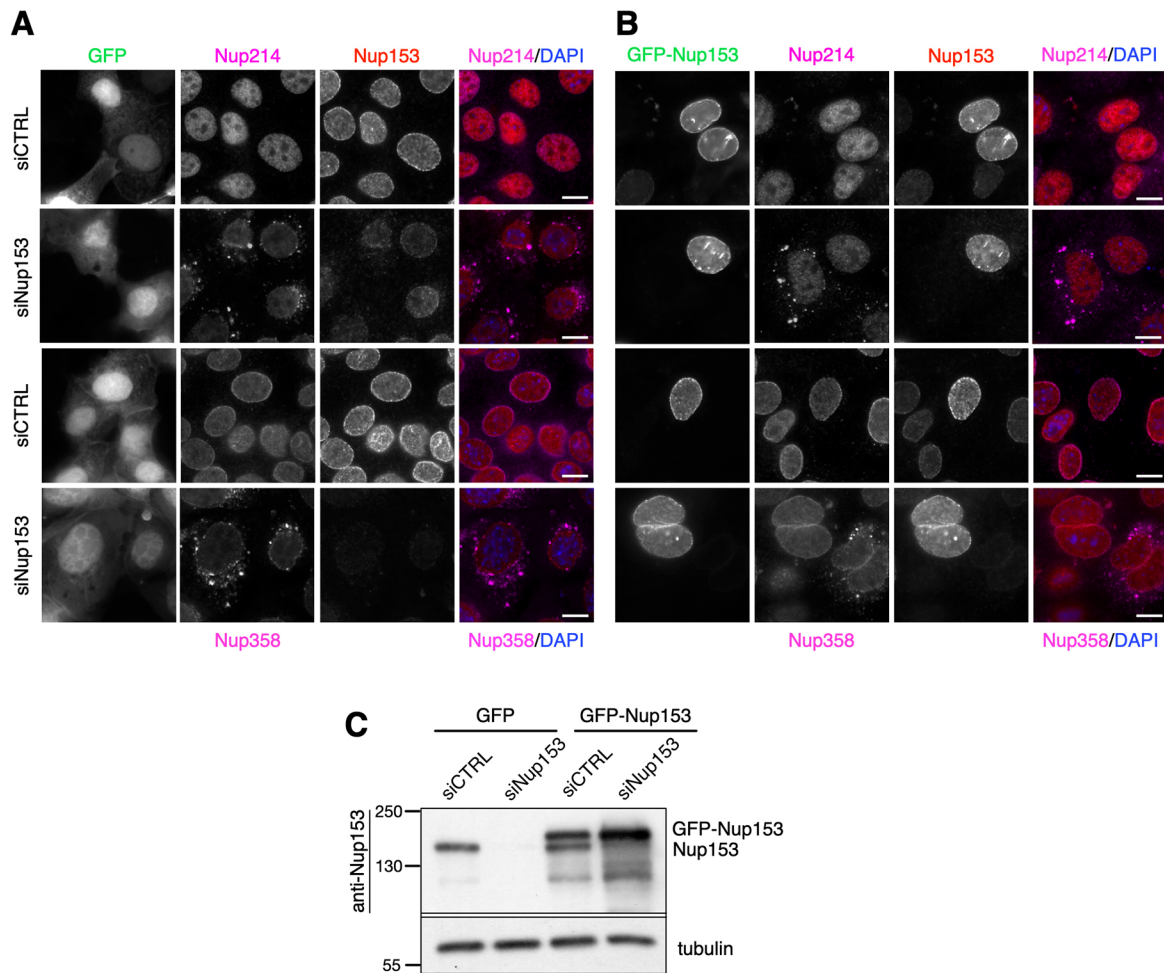
Fig. 6. GFP–Nup153 restores the localisation of cytoplasmic nucleoporins in Nup153-depleted cells. Mouse 3T3 cells were treated with control (siCTRL) and Nup153 siRNAs for 48 h, transfected with (A) GFP or (B) GFP–Nup153 for 24 h, fixed and stained with anti-Nup214 (top) or anti-Nup358 (bottom) antibodies (magenta), and co-stained with anti-Nup153 antibodies (red). The localisation of Nup214 and Nup358 is restored in Nup153-depleted cells expressing RNAi-resistant GFP–Nup153. Epifluorescence images are shown. DNA is stained with DAPI (blue). Scale bars: 10 µm. (C) Western blot analysis showing the expression of Nup153 in total cell protein lysates from control (siCTRL) or Nup153-depleted cells expressing GFP or GFP–Nup153. Anti-α-tubulin antibodies were employed as a loading control.

the Mad2-interacting motif (MIM; Fig. 1), in agreement with the previously published observation that Mad2 does not co-purify with the Nup153–Mad1 complex (Lussi et al., 2010). Along these lines, and consistent with previous studies (Lussi et al., 2010; Mackay et al., 2009, 2010), depletion of Nup153 had no obvious impact on the SAC (Fig. S2), in contrast to the effects of depletion of the Tpr–Mad1 complex (Lee et al., 2008; Schweizer et al., 2013). Furthermore, our PLA experiments revealed that Nup153 and Mad1 bind each other exclusively in the presence of the NE, from late telophase to early prophase (Fig. 2C). We confirmed that Nup153 and Mad1 do not colocalise to kinetochores during prometaphase (Lussi et al., 2010; Mackay et al., 2010), therefore we consider it highly unlikely that Nup153 and Mad1 act together in SAC control.

Surprisingly, Mad1 depletion led to delayed recruitment of Nup153 to chromatin in anaphase, coinciding with a prolonged anaphase (Fig. 3D). At this stage we do not know whether Mad1 directly targets Nup153 to chromatin or whether it bridges another factor. A complex between Repo-Man and importin β is known to be important for targeting Nup153 to anaphase chromatin (Vagnarelli and Earnshaw, 2012; Vagnarelli et al., 2011). Lack of

Repo-Man impairs importin β recruitment and subsequent recruitment of Nup153 to the anaphase chromatin. Whether Repo-Man docks to the chromatin directly or indirectly remains unclear (Vagnarelli and Earnshaw, 2012). Repo-Man also targets protein phosphatase 1γ (PP1γ) to chromatin in anaphase and regulates chromosome remodelling during the late stages of mitosis. When PP1γ is absent, anaphase is extended (Axton et al., 1990; Chen et al., 2007), similar to what we observed in Mad1-depleted cells (Fig. 3D). Delayed recruitment of Nup153 in Mad1-depleted cells might therefore arise from a perturbed Repo-Man–PP1γ localisation or function. Although we did not observe a mislocalisation of importin β in Mad1-depleted cells (Fig. S4A), a Repo-Man-mediated effect of Mad1 on Nup153 cannot be completely ruled out. Alterations in short-lived dynamic processes such as recruitment to chromatin during anaphase might be missed in fixed samples, and it would require in-depth time-lapse imaging to monitor localisation of Repo-Man and PP1γ on chromatin during anaphase in Mad1-depleted cells.

What is the consequence of failed recruitment of Nup153 to anaphase chromatin? At first sight, relatively little. Although Nup153 acts as seed for NPC assembly (Schwartz et al., 2015), it is
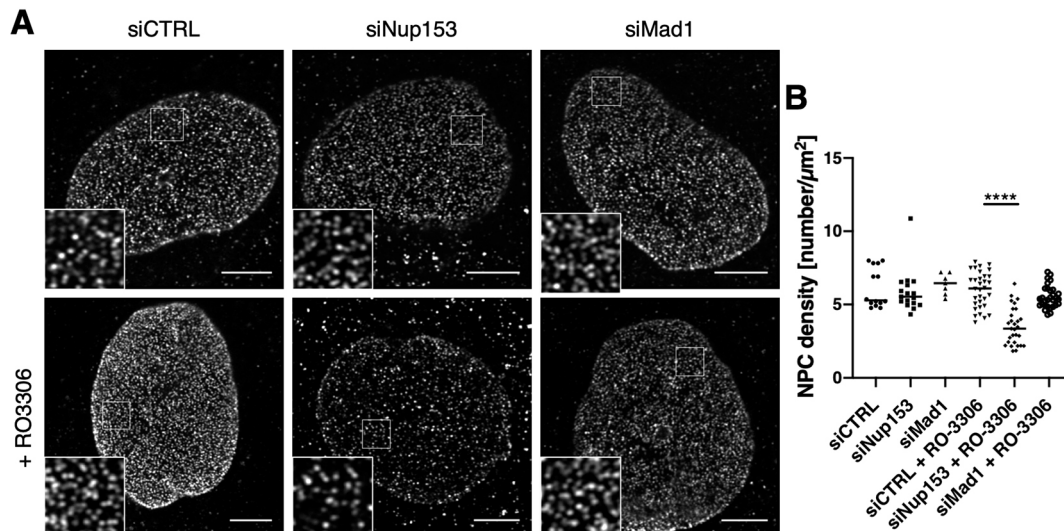
Fig. 7. NPC density is reduced in Nup153-depleted cells. (A) HeLa cells were transfected with the indicated siRNAs (siCTRL, control non-targeting siRNA) and, at 48 h post transfection, treated with RO-3306 (+RO3306) for 18 h to induce a G2-M arrest. NPCs were visualised using mAb414 antibodies. Representative confocal images taken in combination with a Zeiss Airyscan detector are shown. Inset images show higher magnification of the marked areas in the overview images. Scale bars: 5 μm. (B) Quantification of NPC density on the nuclear surface for the indicated conditions, using the ImageJ cell counter plugin. Horizontal lines indicate means. ****$P<0.0001$ (one-way ANOVA).

not the only seeding nucleoporin. Nup133, ELYS and Nup50 are equally capable of seeding NPCs (Schwartz et al., 2015), indicating a highly secured mechanism that ensures faithful post-mitotic NPC assembly and that does not depend on a sole nucleoporin. At a closer look, however, Mad1- and Nup153-depleted cells showed prominent ultrastructural changes in membrane curvature at the NPC–NE interface (Fig. 4A,B) and in NE spacing (Fig. 4A–D). Indeed, the yeast orthologue of Nup153, Nup1, is required for correct membrane curvature due to the presence of an N-terminal amphipathic helix (Meszaros et al., 2015), and Nup153 similarly contains such an amphipathic helix in its N terminus (Vollmer et al., 2015). Via their amphipathic helices, both these nucleoporins are capable of directly interacting with liposomes *in vitro* and inducing liposome tubulation (Meszaros et al., 2015; Vollmer et al., 2015), suggesting that the amphipathic helix of Nup153s is an evolutionarily conserved necessity for correct membrane curvature at NPCs. Similarly, other nucleoporins containing amphipathic helices, such as Nup155, Nup133 and Nup53 (also known as NUP35) are capable of inducing membrane curvature (Drin et al., 2007; Kim et al., 2014; Schwartz, 2016; Vollmer et al., 2012). The expansion of the spacing between ONM and INM is likely caused by an increase in the tension between lipids in the NE, which is normally attenuated by amphipathic helices, such as the one in Nup153. Proteins forming LINC complexes to connect the cytoplasm to the nucleoplasm have also been implicated in NE spacing: SUN (Sad1 and UNC-84) proteins in the INM and KASH (Klarsicht, ANC-1 and Syne homology) proteins in the ONM (Crisp et al., 2006). SUN proteins, however, have been shown to not dictate the width of the NE, and SUN–KASH bridges are only required to maintain NE spacing in cells subjected to increased mechanical forces (Cain et al., 2014). Consistent with this, we observed a regular localisation of both SUN and KASH proteins in the NE of Nup153- and Mad1-depleted cells (Fig. S6C).

Do these membrane curvature and NE spacing abnormalities reflect post-mitotic or interphase assembly defects? We consider it likely that they are post-mitotic defects, because defects in interphase assembly would lead to membrane collapse rather than membrane expansion, as described for POM121 (Talamas and

Hetzer, 2011). Furthermore, the depletion of Nup153 led to a displacement of the cytoplasmic nucleoporins Nup358, Nup214 and Nup88 (Figs 5, 6), as well as to reduced NPC density after S phase (Fig. 7). Partial mislocalisation of cytoplasmic nucleoporins to NPCs is also seen in Nup1-depleted yeast cells (Meszaros et al., 2015). NPC assembly in yeast occurs exclusively into a closed NE, strongly suggesting that the displacement of the cytoplasmic nucleoporins in cells lacking Nup153 is due to interphase NPC assembly defects. It is conceivable that newly synthesised cytoplasmic nucleoporins cannot incorporate into NPCs during the G2 phase of the cell cycle, when the NE is expanding after DNA replication (Makio et al., 2009; Meszaros et al., 2015; Vollmer et al., 2015). Displacement of cytoplasmic nucleoporins and a reduction in NPC density was not observed in Mad1-depleted cells, suggesting that Nup153 acts independently of Mad1 in interphase NPC assembly. Taken together our data therefore suggest that Nup153 has separable roles in post-mitotic NE formation in concert with Mad1 and in interphase NPC assembly independently of Mad1. Whether the role of Mad1 in post-mitotic NE re-formation is solely to its role in Nup153 recruitment to anaphase chromatin remains to be elucidated.

MATERIALS AND METHODS
All experiments were carried out at room temperature, unless otherwise stated.

Cell culture and transfections
HeLa cells and 3T3 cells were grown in Dulbecco's modified Eagle's medium (DMEM) supplemented with 10% foetal bovine serum (FBS; Biochrom GmbH, Berlin, Germany), 100 U/ml penicillin (Thermo Fisher Scientific, Invitrogen, Waltham, MA, USA) and 100 U/ml streptomycin (Invitrogen) and maintained at 37°C in a humidified incubator with 5% CO_2. HeLa cells stably expressing YFP–tubulin were grown in DMEM containing 10% FBS, penicillin, streptomycin and 250 μg/ml geneticin (G418).

HeLa T-Rex cells expressing GFP–Nup98 were established by transfection with pcDNA4/TO-GFP-NUP98 (a kind gift from Dr. Vincent Duheron, Université Libre de Bruxelles, Belgium), and positive clones were selected by treatment with 5 mg/ml blasticidin and 200 mg/ml zeocin. Individual clones were isolated, expanded and cultured in MEM (Life

Technologies Gibco, Gent, Belgium) containing 10% FBS, blasticidin, zeocin, penicillin and streptomycin. HeLa T-Rex cells expressing GFP–Nup153 (Duheron et al., 2014) or GFP–Nup98 were grown in Minimal Essential Medium (MEM) containing 10% FBS, penicillin, streptomycin, 5 μg/ml blasticidin (Invitrogen) and 200 μg/ml zeocin (Invivogen, Toulouse, France). Cells were treated with 1 μg/ml of tetracycline (Sigma-Aldrich, Machelen, Belgium) for 24 h to induce the expression of GFP–Nup153 or GFP–Nup98. Cells were tested for mycoplasma contamination on a regular basis (MycoAlert detection kit; Lonza, Basel, Switzerland).

Cells were transfected using Lipofectamine RNAiMAX (Invitrogen) for siRNAs and Lipofectamine 2000 (Invitrogen) for plasmids, according to the instructions of the manufacturer. The siRNAs used were On-target plus smart pool siRNAs purchased from Dharmacon (Lafayette, CO, USA): non-targeting siRNAs (D-001810-10), human Nup153 siRNAs (L-005283-00), human Tpr siRNAs (L-010548-00), human Mad1 siRNAs (L-006825-00), human Mad2 siRNAs (L-003271-00), mouse cyclophilin B control (D-001820-02), mouse Nup153 siRNAs (L-057025-01).

To arrest cells at the G2-M boundary, cells were treated with 9 μM RO-3306 (Sigma-Aldrich) for 18 h.

Constructs
For the generation of pGEX-6P-Nup153, human *NUP153* was amplified by PCR and inserted into XhoI/NotI cut pGEX-6P (GE Life Sciences, Darmstadt, Germany). For the generation of pEGFP–Nup153, PCR-amplified human *NUP153* was inserted into HindIII/XmaI cut pEGFP-C3 (Takara Bio Europe/Clontech, Saint-Germain-en-Laye, France). For all Mad1 constructs, human *MAD1* was amplified by PCR. Recombinant full-length FLAG–Mad1 and FLAG–Mad1-N596 were subcloned from pFLAG-CMV2-Mad1 (Lussi et al., 2010) into NheI/BamHI cut pET24d+ (EMD Biosciences, Darmstadt, Germany). The other fragments were generated by adding an N-terminal FLAG-tag into the forward primers. The resulting products were subcloned into NheI/BamHI cut pET24d+. All the constructs were verified by DNA sequencing. All primers are listed in Table S1.

Antibodies
Primary antibodies used were: monoclonal mouse anti-Nup153, clone SA1 [hybridoma supernatant; a kind gift from Dr Brian Burke, A* STAR Biomedical Sciences Cluster, Singapore; immunofluorescence (IF) 1:100, western blot (WB) 1:50]; mouse anti-Mad1 (Santa Cruz, Heidelberg, Germany; sc-47746; IF 1:100, WB 1:1000); mouse anti-Tpr (Abnova, Hamm, Germany; H00007175-M01; IF 1:400, WB 1:2000); mouse anti-Mad2 (Sigma-Aldrich; M8694; WB 1:1000); mouse anti-laminA/C (Abcam, Cambridge, UK; ab40567; IF 1:60); mouse anti-FLAG (Sigma-Aldrich; F3165; WB 1:2000); mouse anti-Hec1 (Abcam; ab3613; IF 1:200); mouse mAb414 (Covance, Mechelen, Belgium; IF 1:5000); mouse anti-importin β (BD Biosciences, Erembodegem, Belgium; 610559; IF 1:1000); polyclonal rabbit anti-Nup153 (Sigma-Aldrich; HPA027896; IF 1:400); rabbit anti-Mad1 (Santa Cruz; sc-67338; IF 1:100); rabbit anti-Mad2 (Covance; PRB-452C; IF 1:200); rabbit anti-α-tubulin (Abcam; ab18251; WB 1:4000); rabbit anti-actin (Sigma-Aldrich; A2066; WB 1:1000); rabbit anti-Nup88 (BD Biosciences; 611896; IF 1:500); rabbit anti-nesprin 2 (a kind gift from Dr Iakowos Karakesisoglou, University of Durham, UK; IF 1:300); rabbit anti-Sun1 (a kind gift from Dr Ulrike Kutay, ETH Zurich, Switzerland; IF 1:1000); rabbit anti-Nup214 (a kind gift from Dr Ralph Kehlenbach, University of Göttingen, Germany; IF 1:1000); and rabbit anti-Nup358 (a kind gift from Dr Mary Dasso, National Institutes of Health, Bethesda, MD, USA; IF 1:300).

Secondary antibodies for immunofluorescence were: goat anti-mouse IgG–Alexa 488, goat anti-rabbit IgG–Alexa 488, goat anti-mouse IgG–Alexa 568, goat anti-rabbit IgG–Alexa 568 and chicken anti-mouse IgG–Alexa 647 from Molecular Probes (Paisley, UK). All antibodies were used at a dilution of 1:1000. For western blotting, secondary goat anti-mouse IgG and goat anti-rabbit coupled with alkaline phosphatase antibodies (Sigma-Aldrich) were used at a dilution of 1:20,000.

GST pulldown assays
All recombinant FLAG–Mad1 fragments, GST, and GST–Nup153N were produced in *E. coli* BL21 codon plus (DE3) cells. Bacteria precultures were

grown overnight at 37°C in 1 ml LB medium containing appropriate antibiotics and diluted into 100 ml LB medium containing appropriate antibiotics. Protein expression was induced with 0.1 mM of isopropyl-beta-D-thiogalactopyranoside (IPTG) at an optical density at 600 nm of 0.5, and cells were grown for a further 3 h at 37°C. The cells were collected by centrifugation at 4°C at 3220 *g* for 20 min, resuspended in 4 ml phosphate-buffered saline (PBS) containing 1% Triton X-100 plus protease inhibitor cocktail (Roche, Basel, Switzerland) and then sonicated on ice (five times for 10 s, with 10 s off between each sonication). After centrifugation at 4°C at 16,000 *g* for 15 min, the supernatants were collected, frozen in liquid nitrogen and stored at −80°C.

For pulldown assays, 500 μl of GST or 200 μl of GST–Nup153N were bound to 20 μl of glutathione–sepharose beads (Fig. S1) for 1 h at 4°C on a rocker platform. Next, the beads were washed twice with PBS containing 1% Triton X-100 and a cocktail of protease inhibitors and subsequently twice with 50 mM HEPES, pH 7.4, 150 mM NaCl, 1 mM DTT, 0.1% NP-40 and protease inhibitors. The beads were next incubated with the different recombinant FLAG–Mad1 fragments for 1 h at 4°C on a rocker platform. After binding, beads were washed four times with 50 mM HEPES, pH 7.4, 150 mM NaCl, 1 mM DTT, 0.1% NP-40, then resuspended in 2× Laemmli buffer (125 mM Tris-HCl, pH 6.8, 4% SDS, 20% glycerol, 10% 2-mercaptoethanol and 0.004% Bromophenol Blue) and boiled for 5 min at 95°C. Next, the samples were separated by SDS–PAGE and analysed by western blotting.

Immunofluorescence microscopy
Cells were grown on glass coverslips and fixed with 2% formaldehyde for 15 min. Next, cells were washed three times with PBS for 5 min and permeabilised with PBS containing 0.2% Triton X-100 and 1% bovine serum albumin (BSA) for 10 min. After three washes with PBS containing 1% BSA for 5 min, cells were stained with the appropriate antibodies for 2 h at room temperature or overnight at 4°C in a humid chamber. Next, cells were washed three times with PBS containing 1% BSA, incubated with secondary antibodies for 1 h and washed four times with PBS. The coverslips were then mounted with Mowiol-4088 (Sigma-Aldrich) containing 1 μg/ml DAPI and stored at 4°C until viewed. Images were acquired using a 63× oil immersion objective on a LSM710 laser-scanning confocal microscope (Zeiss, Oberkochen, Germany) or on an Axio Observer Z.1 microscope (Zeiss). Images were recorded with the respective system software and processed using ImageJ (NIH, Bethesda, MD, USA) and Adobe Photoshop.

To visualise importin β at the NE, cells were washed once with PBS and then with ice-cold buffer (20 mM HEPES, pH 7.3, 110 mM potassium acetate, 2 mM magnesium acetate). Next, cells were permeabilised using freshly made ice-cold buffer complemented with 2 mM DTT, protease inhibitor cocktail and 40 μg/ml digitonin. After 5 min incubation on ice, cells were washed twice with PBS and subjected to immunofluorescence as described above.

Fluorescence intensities were measured on images with adjusted threshold using ImageJ.

Proximity ligation assays
Proximity ligation assays were performed according to the instructions of the manufacturer (Duolink; Olink Bioscience, Uppsala, Sweden). HeLa cells were grown on glass coverslips, fixed and permeabilised as described above for immunofluorescence experiments. After incubation with primary antibodies, the cells were subjected to the Duolink red kit. After washing with Duolink wash buffer A, cells were incubated with the Duolink PLA probes for 1 h at 37°C in a pre-heated humidified chamber. Following washing steps with Duolink wash buffer A, the Duolink ligation reagent was incubated for 30 min followed by the Duolink amplification reagent for 90 min, both at 37°C in a pre-heated humidified chamber. Cells were washed with Duolink wash buffer B and mounted with the Duolink *in situ* mounting medium containing DAPI. Images were acquired using a 63× oil immersion objective on a Zeiss Axio Observer Z.1 fluorescence microscope, recorded with Axiovison software and processed using ImageJ and Adobe Photoshop.

Time-lapse imaging
HeLa T-Rex were grown in CELLview glass-bottomed cell culture chambers (Greiner Bio-One, Kremsmünster, Austria), transiently treated

with siRNAs for 48 h and maintained at 37°C in complete MEM medium. Next, to induce expression of GFP–Nup153 or GFP–Nup98, cells were treated with tetracycline at a final concentration of 1 µg/ml for 24 h. Cells were equilibrated in a CO_2-independent medium without Phenol Red (Leibovitz's L-15 medium; Gibco) supplemented with 10% FBS, penicillin, streptomycin and L-glutamine. About 2 h after medium exchange, cells were placed into a 37°C pre-heated incubation chamber. Time-lapse sequences were recorded every minute for ~1 h. Images were taken using a 63×/1.4 oil immersion objective lens on an LSM710 laser-scanning confocal microscope (Zeiss) and were recorded using the system software. The images were processed with ImageJ and Adobe Photoshop.

Super-resolution 3D structured illumination microscopy
HeLa cells were grown on glass coverslips and treated with siRNAs for 48 h, then subjected to immunofluorescence as described above. The coverslips were mounted using Vectashield 1000 and sealed with nail polish. For acquisition, the 488 nm and 568 nm laser lines were used. Images were taken on a DeltaVision OMX Blaze version 4 microscope (Applied Precision, Issaquah, WA). The images were processed and reconstructed with the DeltaVision OMX SoftWoRx software package (Applied Precision).

Electron microscopy
HeLa T-Rex cells were grown in 6-well plates and treated with the respective siRNAs and maintained in 5% CO_2 at 37°C in MEM. 48 h after transfection (72 h for Tpr siRNAs), cells were collected using a cell scraper, pelleted and washed once with PBS. Cells were fixed for 1 h in Karnovsky solution (10 mM PBS, pH 7.4, 3% paraformaldehyde and 0.5% glutaraldehyde) and washed once with PBS. Post-fixation was performed in 1% reduced osmium tetroxide containing 1.5% potassium ferricyanide for 40 min and 1% osmium tetroxide for another 40 min. Cells were washed with water, and samples were next dehydrated in a series of ethanol solutions, embedded in Epon resin, and subjected to EM analysis. EM micrographs were taken on a Phillips CM-100 transmission electron microscope equipped with a CCD camera, at an acceleration voltage of 80 kV. Images were recorded using the system software and processed using Adobe Photoshop.

Western blotting
Cells were harvested by trypsinisation, washed with PBS and resuspended in lysis buffer [50 mM Tris-HCl, pH 7.5, 150 mM NaCl, 1% NP-40 supplemented with a protease inhibitor cocktail (Roche, Basel, Switzerland)] then incubated for 15 min at 4°C. Subsequently, the lysates were cleared by centrifugation at 16,000 g at 4°C for 10 min. The lysates were resuspended in Laemmli buffer and boiled for 5 min at 95°C. 20 µg of protein was then separated by SDS–PAGE for 90 min at 100 V, and the proteins were transferred onto a PVDF membrane using a current of 20 mA overnight. Next, the membrane was incubated for 1 h in Tris-buffered saline (TBS) containing 0.1% Tween 20 (TBS-T) and 5% non-fat dry milk, followed by incubation of primary antibodies in the blocking solution for 2 h at room temperature or overnight at 4°C. After washing three times with TBS-T, the membrane was incubated with the appropriate alkaline phosphatase-conjugated secondary antibody for 1 h. After three washes with TBS-T, the membrane was washed twice with assay buffer (100 mM Tris-HCl, pH 9.8, 10 mM $MgCl_2$) for 2 min. The membrane was incubated for 5 min with the Lightning CDP Star chemiluminescence reagent (Thermo Fisher Scientific, Applied Biosystems) and exposed on CL-Xposure film (Thermo Fisher Scientific).

Nocodazole arrest and spindle assembly checkpoint analysis
Cells were grown in 6-well plates and transiently treated with siRNAs. 24 h post transfection, cells were treated with 2 mM thymidine (Sigma-Aldrich) for 24 h, washed with PBS, released into fresh medium for 3 h, and treated with 100 ng/ml nocodazole (Sigma-Aldrich) for 12 h. Cells were next released into fresh medium for 0, 45, 90, 120 or 150 min before being lysed in lysis buffer [50 mM Tris-HCl, pH 7.5, 150 mM NaCl, 1% NP-40 supplemented with a protease inhibitor cocktail (Roche)] and subjected to western blot analysis.

Supplementary information
Supplementary information available online at
https://jcs.biologists.org/lookup/doi/10.1242/jcs.249243.supplemental

Peer review history
The peer review history is available online at
https://jcs.biologists.org/lookup/doi/10.1242/jcs.249243.reviewer-comments.pdf

References
Anderson, D. J., Vargas, J. D., Hsiao, J. P. and Hetzer, M. W. (2009). Recruitment of functionally distinct membrane proteins to chromatin mediates nuclear envelope formation in vivo. J. Cell Biol. 186, 183-191. doi:10.1083/jcb.200901106

Axton, J. M., Dombrádi, V., Cohen, P. T. W. and Glover, D. M. (1990). One of the protein phosphatase 1 isoenzymes in Drosophila is essential for mitosis. Cell 63, 33-46. doi:10.1016/0092-8674(90)90286-N

Ball, J. R. and Ullman, K. S. (2005). Versatility at the nuclear pore complex: lessons learned from the nucleoporin Nup153. Chromosoma 114, 319-330. doi:10.1007/s00412-005-0019-3

Beck, M. and Hurt, E. (2017). The nuclear pore complex: understanding its function through structural insight. Nat. Rev. Mol. Cell Biol. 18, 73-89. doi:10.1038/nrm.2016.147

Bilir, Ş., Kojidani, T., Mori, C., Osakada, H., Kobayashi, S., Koujin, T., Hiraoka, Y. and Haraguchi, T. (2019). Roles of Nup133, Nup153 and membrane fenestrations in assembly of the nuclear pore complex at the end of mitosis. Genes Cells 24, 338-353. doi:10.1111/gtc.12677

Boehmer, T., Enninga, J., Dales, S., Blobel, G. and Zhong, H. (2003). Depletion of a single nucleoporin, Nup107, prevents the assembly of a subset of nucleoporins into the nuclear pore complex. Proc. Natl. Acad. Sci. USA 100, 981-985. doi:10.1073/pnas.252749899

Cain, N. E., Tapley, E. C., McDonald, K. L., Cain, B. M. and Starr, D. A. (2014). The SUN protein UNC-84 is required only in force-bearing cells to maintain nuclear envelope architecture. J. Cell Biol. 206, 163-172. doi:10.1083/jcb.201405081

Campbell, M. S., Chan, G. K. and Yen, T. J. (2001). Mitotic checkpoint proteins HsMAD1 and HsMAD2 are associated with nuclear pore complexes in interphase. J. Cell Sci. 114, 953-963.

Chen, R.-H., Shevchenko, A., Mann, M. and Murray, A. W. (1998). Spindle checkpoint protein Xmad1 recruits Xmad2 to unattached kinetochores. J. Cell Biol. 143, 283-295. doi:10.1083/jcb.143.2.283

Chen, F., Archambault, V., Kar, A., Lio', P., D'Avino, P. P., Sinka, R., Lilley, K., Laue, E. D., Deak, P., Capalbo, L. et al. (2007). Multiple protein phosphatases are required for mitosis in Drosophila. Curr. Biol. 17, 293-303. doi:10.1016/j.cub.2007.01.068

Crisp, M., Liu, Q., Roux, K., Rattner, J. B., Shanahan, C., Burke, B., Stahl, P. D. and Hodzic, D. (2006). Coupling of the nucleus and cytoplasm: role of the LINC complex. J. Cell Biol. 172, 41-53. doi:10.1083/jcb.200509124

Cunha-Silva, S., Osswald, M., Goemann, J., Barbosa, J., Santos, L. M., Resende, P., Bange, T., Ferrás, C., Sunkel, C. E. and Conde, C. (2020). Mps1-mediated release of Mad1 from nuclear pores ensures the fidelity of chromosome segregation. J. Cell Biol. 219, e201906039. doi:10.1083/jcb.201906039

D'Angelo, M. A., Anderson, D. J., Richard, E. and Hetzer, M. W. (2006). Nuclear pores form de novo from both sides of the nuclear envelope. *Science* **312**, 440-443. doi:10.1126/science.1124196

Ding, D., Muthuswamy, S. and Meier, I. (2012). Functional interaction between the Arabidopsis orthologs of spindle assembly checkpoint proteins MAD1 and MAD2 and the nucleoporin NUA. *Plant Mol. Biol.* **79**, 203-216. doi:10.1007/s11103-012-9903-4

Doucet, C. M. and Hetzer, M. W. (2010). Nuclear pore biogenesis into an intact nuclear envelope. *Chromosoma* **119**, 469-477. doi:10.1007/s00412-010-0289-2

Doucet, C. M., Talamas, J. A. and Hetzer, M. W. (2010). Cell cycle-dependent differences in nuclear pore complex assembly in metazoa. *Cell* **141**, 1030-1041. doi:10.1016/j.cell.2010.04.036

Drin, G., Casella, J.-F., Gautier, R., Boehmer, T., Schwartz, T. U. and Antonny, B. (2007). A general amphipathic α-helical motif for sensing membrane curvature. *Nat. Struct. Mol. Biol.* **14**, 138-146. doi:10.1038/nsmb1194

Duheron, V., Chatel, G., Sauder, U., Oliveri, V. and Fahrenkrog, B. (2014). Structural characterization of altered nucleoporin Nup153 expression in human cells by thin-section electron microscopy. *Nucleus* **5**, 601-612. doi:10.4161/19491034.2014.990853

Duheron, V., Nilles, N., Pecenko, S., Martinelli, V. and Fahrenkrog, B. (2017). Localisation of Nup153 and SENP1 to nuclear pore complexes is required for 53BP1-mediated DNA double-strand break repair. *J. Cell Sci.* **130**, 2306-2316. doi:10.1242/jcs.198390

Dultz, E., Zanin, E., Wurzenberger, C., Braun, M., Rabut, G., Sironi, L. and Ellenberg, J. (2008). Systematic kinetic analysis of mitotic dis- and reassembly of the nuclear pore in living cells. *J. Cell Biol.* **180**, 857-865. doi:10.1083/jcb.200707026

Fahrenkrog, B., Maco, B., Fager, A. M., Köser, J., Sauder, U., Ullman, K. S. and Aebi, U. (2002). Domain-specific antibodies reveal multiple-site topology of Nup153 within the nuclear pore complex. *J. Struct. Biol.* **140**, 254-267. doi:10.1016/S1047-8477(02)00524-5

Fernandez, A. G. and Piano, F. (2006). MEL-28 is downstream of the Ran cycle and is required for nuclear-envelope function and chromatin maintenance. *Curr. Biol.* **16**, 1757-1763. doi:10.1016/j.cub.2006.07.071

Franz, C., Walczak, R., Yavuz, S., Santarella, R., Gentzel, M., Askjaer, P., Galy, V., Hetzer, M., Mattaj, I. W. and Antonin, W. (2007). MEL-28/ELYS is required for the recruitment of nucleoporins to chromatin and postmitotic nuclear pore complex assembly. *EMBO Rep.* **8**, 165-172. doi:10.1038/sj.embor.7400889

Harel, A., Orjalo, A. V., Vincent, T., Lachish-Zalait, A., Vasu, S., Shah, S., Zimmerman, E., Elbaum, M. and Forbes, D. J. (2003). Removal of a single pore subcomplex results in vertebrate nuclei devoid of nuclear pores. *Mol. Cell* **11**, 853-864. doi:10.1016/S1097-2765(03)00116-3

Hawryluk-Gara, L. A., Platani, M., Santarella, R., Wozniak, R. W. and Mattaj, I. W. (2008). Nup53 is required for nuclear envelope and nuclear pore complex assembly. *Mol. Biol. Cell* **19**, 1753-1762. doi:10.1091/mbc.e07-08-0820

Hoelz, A., Glavy, J. S. and Beck, M. (2016). Toward the atomic structure of the nuclear pore complex: when top down meets bottom up. *Nat. Struct. Mol. Biol.* **23**, 624-630. doi:10.1038/nsmb.3244

Iouk, T., Kerscher, O., Scott, R. J., Basrai, M. A. and Wozniak, R. W. (2002). The yeast nuclear pore complex functionally interacts with components of the spindle assembly checkpoint. *J. Cell Biol.* **159**, 807-819. doi:10.1083/jcb.200205068

Kim, S. J., Fernandez-Martinez, J., Sampathkumar, P., Martel, A., Matsui, T., Tsuruta, H., Weiss, T. M., Shi, Y., Markina-Inarrairaegui, A., Bonanno, J. B. et al. (2014). Integrative structure-function mapping of the nucleoporin Nup133 suggests a conserved mechanism for membrane anchoring of the nuclear pore complex. *Mol. Cell. Proteomics* **13**, 2911-2926. doi:10.1074/mcp.M114.040915

Knockenhauer, K. E. and Schwartz, T. U. (2016). The nuclear pore complex as a flexible and dynamic gate. *Cell* **164**, 1162-1171. doi:10.1016/j.cell.2016.01.034

Lau, C. K., Delmar, V. A., Chan, R. C., Phung, Q., Bernis, C., Fichtman, B., Rasala, B. A. and Forbes, D. J. (2009). Transportin regulates major mitotic assembly events: from spindle to nuclear pore assembly. *Mol. Biol. Cell* **20**, 4043-4058. doi:10.1091/mbc.e09-02-0152

Lee, S. H., Sterling, H., Burlingame, A. and McCormick, F. (2008). Tpr directly binds to Mad1 and Mad2 and is important for the Mad1-Mad2-mediated mitotic spindle checkpoint. *Genes Dev.* **22**, 2926-2931. doi:10.1101/gad.1677208

Lemaître, C., Fischer, B., Kalousi, A., Hoffbeck, A.-S., Guirouilh-Barbat, J., Shahar, O. D., Genet, D., Goldberg, M., Betrand, P., Lopez, B. et al. (2012). The nucleoporin 153, a novel factor in double-strand break repair and DNA damage response. *Oncogene* **31**, 4803-4809. doi:10.1038/onc.2011.638

Lim, R. Y. H., Ullman, K. S. and Fahrenkrog, B. (2008). Biology and biophysics of the nuclear pore complex and its components. *Int. Rev. Cell Mol. Biol.* **267**, 299-342. doi:10.1016/S1937-6448(08)00632-1

López-Soop, G., Rønningen, T., Rogala, A., Richartz, N., Blomhoff, H. K., Thiede, B., Collas, P. and Küntziger, T. (2017). AKAP95 interacts with nucleoporin TPR in mitosis and is important for the spindle assembly checkpoint. *Cell Cycle* **16**, 947-956. doi:10.1080/15384101.2017.1310350

Lussi, Y. C., Shumaker, D. K., Shimi, T. and Fahrenkrog, B. (2010). The nucleoporin Nup153 affects spindle checkpoint activity due to an association with Mad1. *Nucleus* **1**, 71-84. doi:10.4161/nucl.1.1.10244

Mackay, D. R., Elgort, S. W. and Ullman, K. S. (2009). The nucleoporin Nup153 has separable roles in both early mitotic progression and the resolution of mitosis. *Mol. Biol. Cell* **20**, 1652-1660. doi:10.1091/mbc.e08-08-0883

Mackay, D. R., Makise, M. and Ullman, K. S. (2010). Defects in nuclear pore assembly lead to activation of an Aurora B–mediated abscission checkpoint. *J. Cell Biol.* **191**, 923-931. doi:10.1083/jcb.201007124

Mackay, D. R., Howa, A. C., Werner, T. L. and Ullman, K. S. (2017). Nup153 and Nup50 promote recruitment of 53BP1 to DNA repair foci by antagonizing BRCA1-dependent events. *J. Cell Sci.* **130**, 3347-3359. doi:10.1242/jcs.203513

Makio, T., Stanton, L. H., Lin, C.-C., Goldfarb, D. S., Weis, K. and Wozniak, R. W. (2009). The nucleoporins Nup170p and Nup157p are essential for nuclear pore complex assembly. *J. Cell Biol.* **185**, 459-473. doi:10.1083/jcb.200810029

Maul, G. G., Price, J. W. and Lieberman, M. W. (1971). Formation and distribution of nuclear pore complexes in interphase. *J. Cell Biol.* **51**, 405-418. doi:10.1083/jcb.51.2.405

Mészáros, N., Cibulka, J., Mendiburo, M. J., Romanauska, A., Schneider, M. and Köhler, A. (2015). Nuclear pore basket proteins are tethered to the nuclear envelope and can regulate membrane curvature. *Dev. Cell* **33**, 285-298. doi:10.1016/j.devcel.2015.02.017

Moudry, P., Lukas, C., Macurek, L., Neumann, B., Heriche, J.-K., Pepperkok, R., Ellenberg, J., Hodny, Z., Lukas, J. and Bartek, J. (2012). Nucleoporin NUP153 guards genome integrity by promoting nuclear import of 53BP1. *Cell Death Differ.* **19**, 798-807. doi:10.1038/cdd.2011.150

Nanni, S., Re, A., Ripoli, C., Gowran, A., Nigro, P., D'Amario, D., Amodeo, A., Crea, F., Grassi, C., Pontecorvi, A. et al. (2016). The nuclear pore protein Nup153 associates with chromatin and regulates cardiac gene expression in dystrophic mdx hearts. *Cardiovasc. Res.* **112**, 555-567. doi:10.1093/cvr/cvw204

Otsuka, S. and Ellenberg, J. (2018). Mechanisms of nuclear pore complex assembly - two different ways of building one molecular machine. *FEBS Lett.* **592**, 475-488. doi:10.1002/1873-3468.12905

Panté, N., Thomas, F., Aebi, U., Burke, B. and Bastos, R. (2000). Recombinant Nup153 incorporates in vivo into Xenopus oocyte nuclear pore complexes. *J. Struct. Biol.* **129**, 306-312. doi:10.1006/jsbi.2000.4232

Patel, S. S., Belmont, B. J., Sante, J. M. and Rexach, M. F. (2007). Natively unfolded nucleoporins gate protein diffusion across the nuclear pore complex. *Cell* **129**, 83-96. doi:10.1016/j.cell.2007.01.044

Prunuske, A. J., Liu, J., Elgort, S., Joseph, J., Dasso, M. and Ullman, K. S. (2006). Nuclear envelope breakdown is coordinated by both Nup358/RanBP2 and Nup153, two nucleoporins with zinc finger modules. *Mol. Biol. Cell* **17**, 760-769. doi:10.1091/mbc.e05-06-0485

Rajanala, K., Sarkar, A., Jhingan, G. D., Priyadarshini, R., Jalan, M., Sengupta, S. and Nandicoori, V. K. (2014). Phosphorylation of nucleoporin Tpr governs its differential localization and is required for its mitotic function. *J. Cell Sci.* **127**, 3505-3520. doi:10.1242/jcs.149112

Rasala, B. A., Ramos, C., Harel, A. and Forbes, D. J. (2008). Capture of AT-rich chromatin by ELYS recruits POM121 and NDC1 to initiate nuclear pore assembly. *Mol. Biol. Cell* **19**, 3982-3996. doi:10.1091/mbc.e08-01-0012

Rodriguez-Bravo, V., Maciejowski, J., Corona, J., Buch, H. K., Collin, P., Kanemaki, M. T., Shah, J. V. and Jallepalli, P. V. (2014). Nuclear pores protect genome integrity by assembling a premitotic and Mad1-dependent anaphase inhibitor. *Cell* **156**, 1017-1031. doi:10.1016/j.cell.2014.01.010

Sachdev, R., Sieverding, C., Flötenmeyer, M. and Antonin, W. (2012). The C-terminal domain of Nup93 is essential for assembly of the structural backbone of nuclear pore complexes. *Mol. Biol. Cell* **23**, 740-749. doi:10.1091/mbc.e11-09-0761

Schwartz, T. U. (2016). The structure inventory of the nuclear pore complex. *J. Mol. Biol.* **428**, 1986-2000. doi:10.1016/j.jmb.2016.03.015

Schwartz, M., Travesa, A., Martell, S. W. and Forbes, D. J. (2015). Analysis of the initiation of nuclear pore assembly by ectopically targeting nucleoporins to chromatin. *Nucleus* **6**, 40-54. doi:10.1080/19491034.2015.1004260

Schweizer, N., Ferrás, C., Kern, D. M., Logarinho, E., Cheeseman, I. M. and Maiato, H. (2013). Spindle assembly checkpoint robustness requires Tpr-mediated regulation of Mad1/Mad2 proteostasis. *J. Cell Biol.* **203**, 883-893. doi:10.1083/jcb.201309076

Söderberg, O., Gullberg, M., Jarvius, M., Ridderstråle, K., Leuchowius, K. J., Jarvius, J., Wester, K., Hydbring, P., Bahram, F., et al. (2006). Direct observation of individual endogenous protein complexes in situ by proximity ligation. *Nat. Methods* **3**, 995-1000. doi:10.1038/nmeth947

Souquet, B., Freed, E., Berto, A., Andric, V., Audugé, N., Reina-San-Martin, B., Lacy, E. and Doye, V. (2018). Nup133 is required for proper nuclear pore basket assembly and dynamics in embryonic stem cells. *Cell Rep.* **23**, 2443-2454. doi:10.1016/j.celrep.2018.04.070

Talamas, J. A. and Hetzer, M. W. (2011). POM121 and Sun1 play a role in early steps of interphase NPC assembly. *J. Cell Biol.* **194**, 27-37. doi:10.1083/jcb.201012154

Terry, L. J. and Wente, S. R. (2009). Flexible gates: dynamic topologies and functions for FG nucleoporins in nucleocytoplasmic transport. *Eukaryot. Cell* **8**, 1814-1827. doi:10.1128/EC.00225-09

Toda, T., Hsu, J. Y., Linker, S. B., Hu, L., Schafer, S. T., Mertens, J., Jacinto, F. V., Hetzer, M. W. and Gage, F. H. (2017). Nup153 Interacts with Sox2 to enable bimodal gene regulation and maintenance of neural progenitor cells. *Cell Stem Cell* **21**, 618-634.e7. doi:10.1016/j.stem.2017.08.012

Vagnarelli, P. and Earnshaw, W. C. (2012). Repo-Man-PP1: a link between chromatin remodelling and nuclear envelope reassembly. *Nucleus* **3**, 138-142. doi:10.4161/nucl.19267

Vagnarelli, P., Ribeiro, S., Sennels, L., Sanchez-Pulido, L., de Lima Alves, F., Verheyen, T., Kelly, D. A., Ponting, C. P., Rappsilber, J. and Earnshaw, W. C. (2011). Repo-Man coordinates chromosomal reorganization with nuclear envelope reassembly during mitotic exit. *Dev. Cell* **21**, 328-342. doi:10.1016/j.devcel.2011.06.020

Vaquerizas, J. M., Suyama, R., Kind, J., Miura, K., Luscombe, N. M. and Akhtar, A. (2010). Nuclear pore proteins nup153 and megator define transcriptionally active regions in the *Drosophila* genome. *PLoS Genet.* **6**, e1000846. doi:10.1371/journal.pgen.1000846

Vollmer, B. and Antonin, W. (2014). The diverse roles of the Nup93/Nic96 complex proteins - structural scaffolds of the nuclear pore complex with additional cellular functions. *Biol. Chem.* **395**, 515-528. doi:10.1515/hsz-2013-0285

Vollmer, B., Schooley, A., Sachdev, R., Eisenhardt, N., Schneider, A. M., Sieverding, C., Madlung, J., Gerken, U., Macek, B. and Antonin, W. (2012). Dimerization and direct membrane interaction of Nup53 contribute to nuclear pore complex assembly. *EMBO J.* **31**, 4072-4084. doi:10.1038/emboj.2012.256

Vollmer, B., Lorenz, M., Moreno-Andrés, D., Bodenhöfer, M., De Magistris, P., Astrinidis, S. A., Schooley, A., Flötenmeyer, M., Leptihn, S. et al. (2015). Nup153 recruits the Nup107-160 complex to the inner nuclear membrane for interphasic nuclear pore complex assembly. *Dev. Cell* **33**, 717-728. doi:10.1016/j.devcel.2015.04.027

Walther, T. C., Fornerod, M., Pickersgill, H., Goldberg, M., Allen, T. D. and Mattaj, I. W. (2001). The nucleoporin Nup153 is required for nuclear pore basket formation, nuclear pore complex anchoring and import of a subset of nuclear proteins. *EMBO J.* **20**, 5703-5714. doi:10.1093/emboj/20.20.5703

Walther, T. C., Alves, A., Pickersgill, H., Loïodice I., Hetzer, M., Galy, V., Hülsmann, B. B., Köcher, T., Wilm, M., et al. (2003). The conserved Nup107-160 complex is critical for nuclear pore complex assembly. *Cell* **113**, 195-206. doi:10.1016/S0092-8674(03)00235-6

Wei, R. R., Sorger, P. K. and Harrison, S. C. (2005). Molecular organization of the Ndc80 complex, an essential kinetochore component. *Proc. Natl. Acad. Sci. USA* **102**, 5363-5367. doi:10.1073/pnas.0501168102

Zhou, L. and Panté, N. (2010). The nucleoporin Nup153 maintains nuclear envelope architecture and is required for cell migration in tumor cells. *FEBS Lett.* **584**, 3013-3020. doi:10.1016/j.febslet.2010.05.038